Full Paper

Wiley Online Library

ELECTROANALYSIS

DOI: 10.1002/elan.201800656

An Enzyme-free H_2O_2 Sensor Based on Poly(2-Aminophenylbenzimidazole)/Gold Nanoparticles Coated Pencil Graphite Electrode

Mine Şen Teker,[a] Erhan Karaca,[a] Nuran Özçiçek Pekmez,*[a] Uğur Tamer,[b] and Kadir Pekmez[a]

Abstract: A poly(2-aminophenylbenzimidazole)/gold nanoparticles (P2AB/AuNPs) coated disposable pencil graphite electrode (PGE) was fabricated as an enzyme-free sensor for the H_2O_2 determination. P2AB/AuNPs and P2AB were successfully synthesized electrochemically on PGE in acetonitrile for the first time. The coatings were characterized by scanning electron microscopy, X-ray diffraction spectroscopy, Energy-dispersive X-ray spectroscopy, Surface-enhanced Raman spectroscopy, and UV-Vis spectroscopy. AuNPs interacted with P2AB as carrier enhances the electrocatalytic activity towards reduction of H_2O_2. The analytical performance was evaluated in a 100 mM phosphate buffer solution at pH 6.5 by amperometry. The steady state current *vs.* H_2O_2 concentration is linear in the range of 0.06 to 100 mM ($R^2 = 0.992$) with a limit of detection 3.67×10^{-5} M at −0.8 V *vs.* SCE and no interference is caused by ascorbic acid, dopamine, uric acid, and glucose. The examination for the sensitive determination of H_2O_2 was conducted in commercially available hair oxidant solution. The results demonstrate that P2AB/AuNPs/PGE has potential applications as a sensing material for quantitative determination of H_2O_2.

Keywords: Electrochemical sensor · Poly(2-aminophenylbenzimidazole) · Gold nanoparticles · Pencil graphite electrode · Hydrogen peroxide

1 Introduction

Conjugated polymers have arisen as promising materials for the design of electronic devices the significant flexibility in their chemical structures in preparation, high surface area, high electrical conductivity, chemical selectivity, excellent biocompatibility and their redox characteristics [1]. The electrochemical polymerization has many advantages, including control of their morphology, good reproducibility, and stability of the polymer film on electrode surfaces based on the applied polymerization parameters [2]. Benzimidazoles are a class of heterocyclic, aromatic compounds which share a fundamental structural characteristic of six-membered benzene fused to five-membered imidazole. Benzimidazole has great application areas such as antitumor, antibacterial agents and corrosion inhibition. It is also of high interest due to two nitrogens of the amine hydrogen as the donor and the imino nitrogen as the acceptor in fuel cell studies [3]. It was proved that electropolymerization of benzimidazole and substituted benzimidazoles produced electroactive polymers with increasing the conjugation and conductivity of the macromolecule [4]. Polybenzimidazole (PB) is an aromatic polymer with exceptional chemical resistance, excellent mechanical strength, and thermal stability [5]. When doped with acid, it behaves as a proton conductor [6].

Hydrogen peroxide (H_2O_2) detection has practical importance in many fields such as industrial, environmental, waste water treatment, textile, and industries household products, disinfectants, tooth whitening products and hair dyes. Due to its extensive applications, the electrochemical sensing of H_2O_2 has obtained great attention in recent years [7]. For example, a Pt nanoparticle modified Pencil Graphite Electrode (PGE) was prepared for non-enzymatic determination of H_2O_2 in a hair dye oxidation cream by Flow Injection Analysis system [7c]. In the study by Benvidi et al., a voltammetric sensor based on a carbon paste electrode with $CuFe_2O_4$ nanoparticle was designed for the electrocatalytic reduction of H_2O_2 and used for detection of H_2O_2 in milk, green tea, hair dye cream and mouthwash solution samples using DPV technique [7d]. In another study, an amperometric sensor was prepared based on gold nanoparticle-decorated copper cross-linked pectin (CuCP-AuNPs) for H_2O_2 determination in the commercially available clinical lens cleaning solutions. [7b].

Fabricating electrodes with metal nanoparticles for determination H_2O_2 sensors have arisen considerable

[a] M. Ş. Teker, E. Karaca, N. Ö. Pekmez, K. Pekmez
Hacettepe University
Department of Chemistry
06800 Ankara, Turkey
E-mail: npekmez@hacettepe.edu.tr
[b] U. Tamer
Gazi University
Faculty of Pharmacy
Department of Analytical Chemistry
06330 Ankara, Turkey

Supporting information for this article is available on the WWW under https://doi.org/10.1002/elan.201800656

attention in recent studies due to their large surface-to-volume ratio high electrical conductivity and excellent surface reaction activity [8]. Especially gold nanoparticles (AuNPs) could provide a friendly microenvironment and act as the conducting tunnel to achieve the direct electron transfer between substances and electrode surfaces [9]. AuNPs could be synthesized by reducing aqueous $HAuCl_4$ solution with the addition of various reducing agents and stabilizing reagents under different parameters and conditions [10]. The literature reported some AuNPs based non-enzymatic H_2O_2 sensors [11]. The studies continue for the improvement of non-enzymatic H_2O_2 sensor.

There has been no report yet related to polymerization of 2-aminophenyl benzimidazole and also modification with AuNPs in non-aqueous medium without adding reducing or stabilizing agents for use as an H_2O_2 sensor. In the present study, gold nanoparticles functionalized 2 aminophenylbenzimidazole was electropolymerized in acetonitrile on disposable pencil graphite electrode, and poly(2-aminophenylbenzimidazole)/gold nanoparticles (P2AB/AuNPs) coated electrode was examined for amperometric analysis of H_2O_2 for the first time.

2 Experimental

2.1 Materials

2-(2-Aminophenyl)-1H-benzimidazole 97% (2AB), Hydrogen tetrachloroaurate ($HAuCl_4$), tetrabutylammoniumperchlorate (TBAP), acetonitrile (ACN), sodium phosphate monobasic dihydrate ($NaH_2PO_4 \cdot 2H_2O$) sodium phosphate dibasic dihydrate ($Na_2HPO_4 \cdot 2H_2O$) and acetic acid (CH_3COOH) were obtained from Sigma-Aldrich (Taufkirchen, Germany). Hydrogen peroxide 35% (Merck/Germany) was freshly prepared before every use. Perchloric acid ($HClO_4$) from Analar was used. Phosphate buffered saline (PBS, 100 mM) was prepared from $NaH_2PO_4 \cdot 2H_2O$, $Na_2HPO_4 \cdot 2H_2O$ and pH value was adjusted to 6.5 by using CH_3COOH solution. Commercial H_2O_2 hair oxidant (URGO, 3%) was purchased from a local market for real sample analysis. All chemicals were used as received. Double distilled water used throughout the study.

2.2 Methods

Electrochemical measurements were performed with a one compartment glass cell using three electrodes by using cyclic voltammetry (CV), amperometric *i-t* techniques and electrochemical impedance techniques. The working electrode was a disposable graphite electrode (TOMBO 2B with a diameter of 0.9 mm). All leads were used as received. The auxiliary electrodes were Pt wire with a compartment for non-aqueos solutions and bare Pt wire for aqueous solutions. The electrochemical studies were referenced to Ag/AgCl (3.0 M KCl) electrode and saturated calomel electrode (SCE) for non-aqueous, aqueous solutions, respectively. Pencil graphite was used as the working electrode for scanning electron microscopy (SEM), Fourier transform infrared spectroscopy (FTIR), X-ray power diffraction (XRD) and surface enhanced Raman (SERS) measurements. ITO glass electrode (5–15 Ω Delta technologies) was also used as a working electrode for UV-Vis studies. CHI 6011D (CH Instruments) and Emstat3$^+$ were used in electrochemical measurements. Electrochemical impedance spectroscopy (EIS) technique was also used for electrochemical characterization of the electrode surface. The surface morphology and elemental mapping of all samples were characterized using NOVA NANOSEM 650/FEI (USA) and AMETEK-EDAX (USA). XRD pattern was recorded by PANalytical/EMPYREAN (USA) with Cu Kα radiation operating at 45 kV and 40 mA. SERS measurements were performed using a DeltaNu Examiner Raman microscope (Laramie, WY, USA) with a 785-nm laser source. FTIR absorbance spectra were conducted on Thermo Scientific Nicolet iS10 (USA). UV-Vis absorption spectra were collected using a Perkin Elmer Lambda UV-Vis-NIR 750 spectrophotometer over the 400–800 nm range. The dry conductivity values of the polymer were measured using the four-probe measuring technique at room temperature.

3 Results and Discussion

3.1 Preparation and Characterization of P2AB and P2AB/AuNPs Films

3.1.1 Preparation of P2AB and P2AB/AuNPs on Pencil Graphite Electrodes

Poly(2-aminophenylbenzimidazole) (P2AB) films with and without gold nanoparticles (AuNPs) were deposited on pencil graphite electrode (PGE) by applying cyclic voltammetry, scanning between −1.0 and 1.4 V *vs.* Ag|AgCl at a scan rate of 100 mV s^{-1}. The electropolymerization of 2-aminophenylbenzimidazole (2AB) was carried out in an electrochemical cell containing acetonitrile solution of 100 mM TBAP, 100 mM 2AB and 75 mM $HClO_4$. 2AB is oxidized after 0.75 V and recorded a broad peak of about 0.9 V as observed in the first cycle (Figure 1A (a)). The formation and growth of the P2AB can easily be seen in Figure 1A (a). The peak intensity due to the oxidation of 2AB gradually decreases, and the broad peaks between −0.2 V and 0.7 V due to the oxidation and reduction of the film increase in intensity as the film grows. When the 2AB monomer is electropolymerized in the presence of $HAuCl_4$ (10.0 mM) (Figure 1A (b)), the small peak of the oxidation of the monomer in the first cycle is distinguished, and this peak disappears slightly during subsequent cycles. The anodic and cathodic peak characteristics of the polymer are the same that of obtained without $HAuCl_4$ but the peak intensities are higher, and the peak-to-peak separation between 0.7 V and −0.2 V decreases. These findings indicate that the polymer formation occurs much faster in the presence of $HAuCl_4$ and more polymer can be deposited on the PGE. Electrochemical behavior was

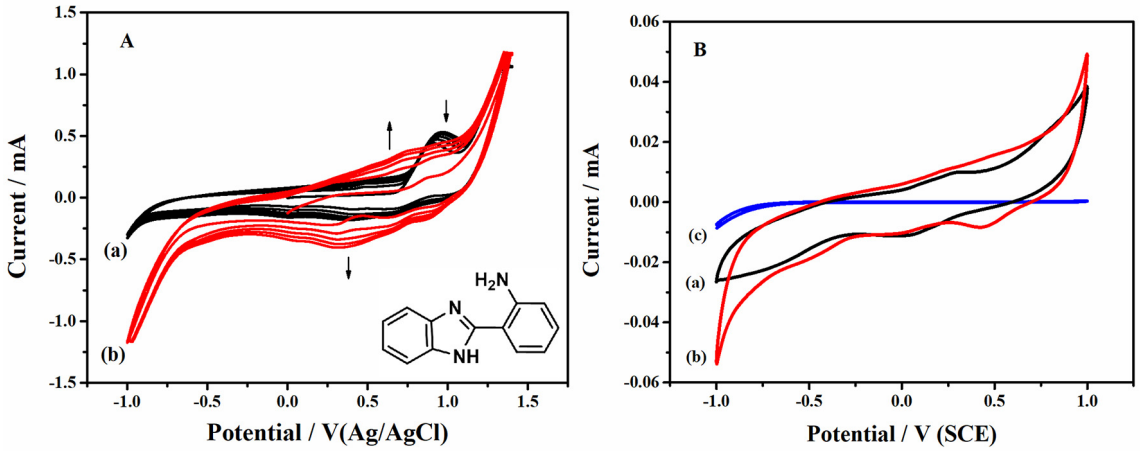

Fig. 1. **(A)** Electrochemical deposition of (a) P2AB and (b) P2AB/AuNPs films by scanning the potential between −1.0 and 1.4 V *vs.* Ag/AgCl on PGE (inset: molecular structure of 2AB). **(B)** Potential cycling curves recorded at 100 mV s^{-1} in PBS pH 6.5 (100 mM) solution for the coatings (a) P2AB, (b) P2AB/AuNPs, and (c) bare pencil graphite electrode, $v = 100$ mV s^{-1}.

investigated for each coated electrode by cyclic voltammetry, scanning between −1.0 V and 1.0 V *vs.* SCE at a scan rate of 100 mV s^{-1} in an aqueous phosphate buffer solution (PBS) of pH 6.5. The redox peak currents of P2AB obtained with a $HAuCl_4$ increase when compared to those of bare and P2AB coated electrodes (Figure 1B (b)). It can be interpreted that AuNPs facilitates the electron transfer process, which means that more polymer deposits on the PGE.

3.1.2 Spectroscopic Characterization

UV-Vis measurements of the polymerization solutions (100 mM TBAP, 100 mM 2AB and 75.0 mM $HClO_4$ in acetonitrile) without and with $HAuCl_4$ (10.0 mM) were performed (Figure S1A (a) and (b)). In the spectrum of the polymerization solution without $HAuCl_4$, an absorbance peak appears at 410 nm (Figure S1A (a)), which is related to π-π electronic interactions. On the other hand, when 10.0 mM $HAuCl_4$ is added to the polymerization solution, light yellow color immediately turns dark violet, and an absorption peak occurs at 535 nm, disappearing the peak at 410 nm (Figure S1A (a)). It is well-known that the peak at 535 nm is the characteristic surface plasmon resonance band of metal nanoparticles [12]. This is the sign of synthesis of the AuNPs. Accordingly, $HAuCl_4$ is reduced to AuNPs in the presence of partially protonated 2AB monomer in acetonitrile solution. In addition, P2AB polymers were deposited on the ITO electrode from the polymerization solutions without and with $HAuCl_4$ by cyclic voltammetry, and their spectra were taken for comparison (Figure S1B). The pale yellow colored P2AB film gives a broad absorption band at 475 nm, while dark yellow colored P2AB/AuNPs film has two absorption bands 485 nm and 555 nm. Comparing the spectra in Figure S1A (a) to B (a), the disappearance of monomer peak (410 nm) and the appearance of a broad peak at 485 nm prove the deposition of P2AB polymer on ITO electrode. The comparison of the spectra in Figure S1A (b) to B (b) shows that the absorption maxima of AuNPs shifts from 535 nm to 555 nm due to electropolymerization of 2AB monomers. Therefore, the peaks at 475 nm and 555 nm in Figure S1B (b) may belong to P2AB moieties without and with AuNPs, respectively.

XRD pattern (Figure S2) was used to further confirmation for the crystal plane of the prepared P2AB/AuNPs film on PGE. In Figure S2, P2AB/AuNPs film characteristic four different diffraction peaks (2θ) at 37.8°, 42.8°, 64.9° and 77.8° are associated with the cubic phase (111, 200, 220, 311) of Au nanoparticles [13]. In addition, the diffraction peaks (2θ) around 42.8°, 54.8° and 77.8° are also corresponding with graphite (101, 004, 103) [14]. The obtained XRD pattern is similar to the previously reported XRD spectra of gold nanoparticles (JCPDS, card no. 04-0784). According to the results, Au nanoparticles and P2AB polymer coexist on the PGE surface.

The FTIR spectroscopy was used to characterize P2AB, and P2AB/AuNPs coated PGEs. The absorbance peaks of P2AB/AuNPs are almost similar to those of P2AB homopolymer (Figure 2A), but it is clear that these bands shift longer wavenumbers. The marked shift may be due to interaction of the P2AB with AuNPs. In the spectrum of P2AB/AuNPs film, a broad band at 3312 cm^{-1} is corresponding to N–H stretching bond [15]. The band at 2900 cm^{-1} is assigned vibrations of aromatic C–H in the polymer chains [16]. The C=N and C=C stretching vibrations of the benzimidazole moiety appear as a broad peak around 1600 cm^{-1} [17]. Also, the peak at 1421 cm^{-1} is ascribed to the ring vibration of the ortho substituted phenyl group [16]. The C–N stretching and N–H bending vibrations of the benzimidazole moiety appear around 1319 and 1361 cm^{-1} [16]. At the peak at 1245 cm^{-1} is assigned to inplane C–H deformation of benzimidazole and phenyl ring [17]. A band at 1030 cm^{-1} may indicate the presence of positive charges in polymer chains and

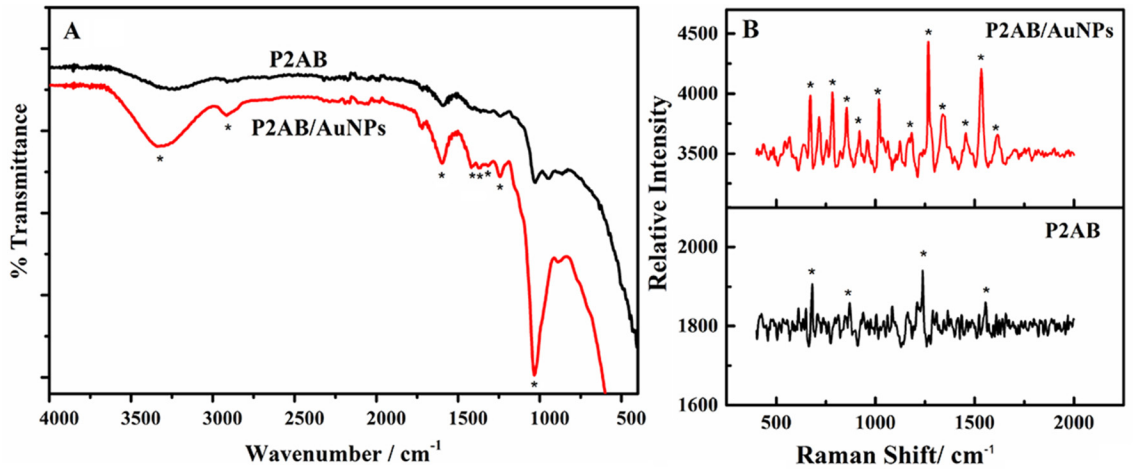

Fig. 2. **(A)** FTIR and **(B)** RAMAN spectra of P2AB and P2AB/AuNPs films on PGE.

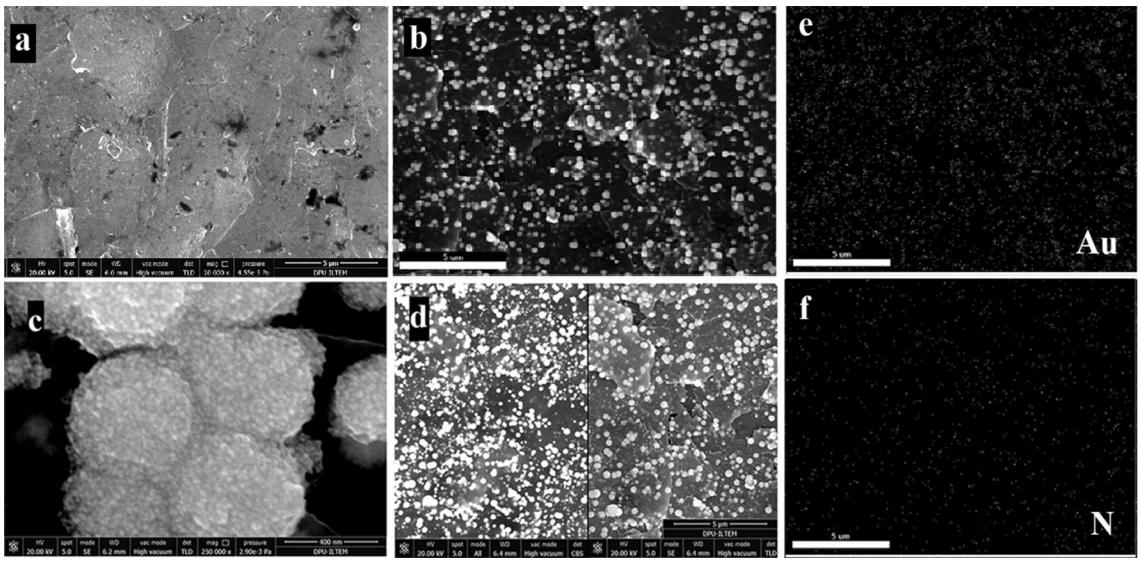

Fig. 3. FE-SEM imaging of (a) P2AB (b,c) P2AB/AuNPs at different magnifications (d) SEM-(BSE and SE) images of P2AB/AuNPs/PGE surface, SEM-EDX mappings of e) gold and f) nitrogen on P2AB/AuNPs/PGE surface.

also assigned to the C–N stretching vibrations of the aminophenyl group [16,18].

The Raman Scattering measurements were carried out to characterize the P2AB, and P2AB/AuNPs coated PGEs (Figure 2B). When compared the spectra of two polymers, the prominent peaks appear in the presence of AuNPs, as expected. In the spectrum of P2AB/AuNPs film, the peak at 958 cm^{-1} is corresponding to ClO_4^- as counter ion [19]. The bands at 673 cm^{-1} assigned to C–C-C out of plane bending, the bands at 787 cm^{-1} and 858 cm^{-1} are corresponding to the C–H out of plane bendings- and the peaks at 1123 cm^{-1} and 1186 cm^{-1} are related to the C–H in plane bending [20]. The C–C aromatic ring chain vibrations observed at 1020 cm^{-1} and 1455 cm^{-1} [20]. Also, the bands occurring at 1266 cm^{-1}, 1345 cm^{-1}, 1534 cm^{-1} and 1620 cm^{-1} are attributed to C–C stretching, the C–N stretching, N–H in-plane bending and C=N vibration of the aromatic ring, respectively [20–21].

3.1.3 SEM-EDX

The morphological structures of the P2AB and P2AB/AuNPs coated PGEs were examined by FE-SEM. As shown in Figure 3 (a), P2AB film exhibits rough surface with a non-uniform distributed defect. On the other hand, the FE-SEM images of P2AB/AuNPs (Figure 3 (b)) show a layered coating with spherical particles, which has sizeable electroactive surface area. The spherical particles may be evidence of Au deposits on the surface of the electrode with the polymer. In order to understand whether or not Au exists, analysis of the surface was carried out by SEM with Backscattered and Secondary Electron (BSE and SE) detectors (Figure 3 (d)) and EDX

Au mapping (Figure 3 (e)). The contrast of Au on the surface can easily be seen in Figure 3 (d). From Figure 3 (e), Au element appears intensively and almost homogeneously, verifying the existence in the coating. Figure 3 (b) shows the cluster size of Au nanoparticles, which are in the range of 30–400 nm. At higher magnification (Figure 3(c)), it is seen that the Au nanoparticles, in the range of 8 to 10 nm, agglomerate as the large gold particles. In addition, the EDX N mapping of P2AB/AuNPs coatings (Figure 3(f)) indicates that the polymer deposited on the electrode surface along with Au nanoparticles.

3.1.4 EIS

Electrochemical impedance spectroscopy (EIS) provides detailed information on the impedance changes of an electrode surface, using an equivalent circuit. Figure 4 and inset show the Nyquist and Bode plots for P2AB homopolymer (Figure 4 (b)) and P2AB/AuNPs composite (Figure 4 (c)) coated PGEs in 100 mM PBS (pH 6.5). To prove the modification of conducting films on PGE, the impedance spectrum of the bare PGE was also recorded (Figure 4 (a)). EIS measurements were fitted using ZSimpWin (Version 3.50). The inset in Figure 4 shows the equivalent circuits used to fit the experimental curves. The fitting values for the equivalent circuit elements and χ^2 values are presented in Table S1. The terms R_s, R_{pore} and R_{ct} refer to the solution resistance, the pore resistance at the electrolyte polymer interface and the charge transfer resistance at the polymer electrode interface, respectively. Q expressed the constant phase element (CPE), which is used in place of double layer capacitance to describe the inhomogeneities [22]. According to Table S1, P2AB coated PGE exhibits ten times lower R_{ct} (and R_{total}) value than that of bare PGE. This is attributed to the fact that the surface of the PGE was successfully modified by conducting polymer. However, R_{pore} (and R_{total}) value of P2AB/AuNPs is ten times higher than that of P2AB coated film. The higher pore resistance may be associated with gold penetration into the pore of compact film.

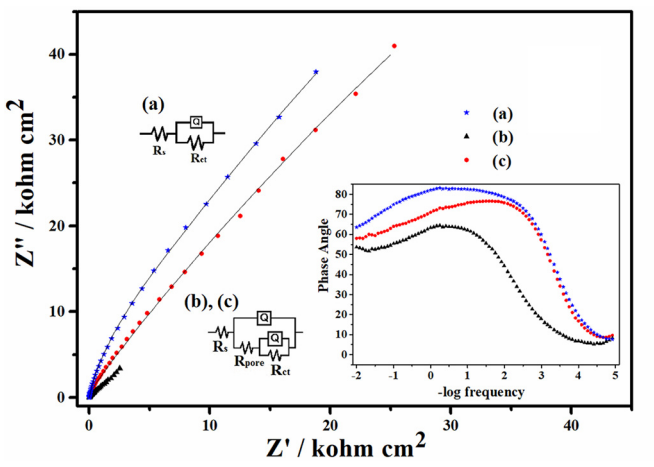

Fig. 4. Nyquist plots obtained in 100 mM PBS solution for coatings of (a) bare PGE and (b) P2AB (c) P2AB/AuNPs coated PGEs (Their Bode plots and equivalent circuits are also shown as inset).

3.1.5 Dry Conductivity

The four-probe technique was used to measure the dry conductivity values of the P2AB and P2AB/AuNPs films at room temperature.The P2AB conductivity value couldn't be measured due to the out of range of the four-probe conductivity device. Alternatively, the conductivity value of P2AB/AuNPs film was determined as 1.3×10^{-4} S/cm. The measurable change in conductivity could be the result of both the presence of Au and the formation of longer chains in the polymer.

3.2 Electrocatalytic Reduction of H_2O_2 at the P2AB/AuNPs/PGE

3.2.1 Electrochemical Behavior of the P2AB/AuNPs/PGE in the Presence of H_2O_2

Electrochemical behaviors of P2AB and P2AB/AuNPs coated electrodes were examined in 100 mM PBS of pH 6.5 containing 1.0 mM H_2O_2 by cyclic voltammetry, scanning between −1,0 V and 1.0 V *vs.* SCE at a scan rate of 100 mV s^{-1}. While the bare electrode does not respond to H_2O_2 (Figure 5A (c)), there is a considerable increase in the reduction peak currents for the coated electrodes. When the redox peaks of coated electrodes are compared with each other, they exhibit almost similar behaviors as seen in Figure 5A (a) and (b), but there is an increase in currents of both oxidation and reduction for P2AB/AuNPs coated electrode (Figure 5A (b)). It is indicated that P2AB polymer in composite film is oxidized with the addition of H_2O_2 in PBS solution while H_2O_2 is reduced. Notably, the reduction current dramatically increases about −0.8 V in the presence of AuNPs. This demonstrates that AuNPs could efficiently catalyze the reduction of H_2O_2 while increasing the conductivity of the P2AB film. According to the literature [23], the mechanism for H_2O_2 electroreduction on the P2AB/AuNPs coated electrode could be expressed as following:

$$H_2O_2 + e^- \rightarrow OH_{ad} + OH^- \quad (1)$$

$$OH_{ad} + e^- \rightarrow OH^- \quad (2)$$

$$2\ OH^- + 2\ H^+ \rightarrow 2\ H_2O \quad (3)$$

Eventually, the modified electrode exhibits higher electrocatalytic activity toward H_2O_2 reduction due to the combination of AuNPs with P2AB.

The effect of scan rates on the electrochemical behavior of P2AB/AuNPs/PGE has been studied in 100 mM PBS of pH 6.5 containing 2.0 mM H_2O_2. The peak currents were measured at varying scan rates from 10–300 mV s^{-1}. As seen in Figure 5B, the cathodic peak

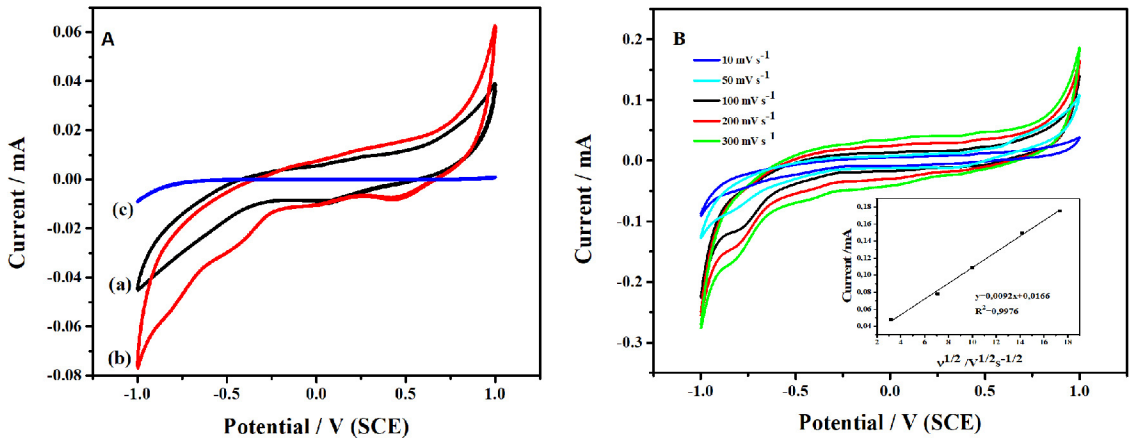

Fig. 5. **(A)** Cyclic voltammograms of (a) P2AB/PGE (b) P2AB/AuNPs/PGE (c) bare PGE in PBS containing 1.0 mM H_2O_2, $v=$ 100 mV s^{-1}. **(B)** Cyclic voltammograms of the P2AB/AuNPs electrode in 100 mM PBS containing 2.0 mM H_2O_2 (pH 6.5) as a function of scan rate (10–300 mV s^{-1}). (inset : Plot of peak currents *vs.* the square root of scan rate).

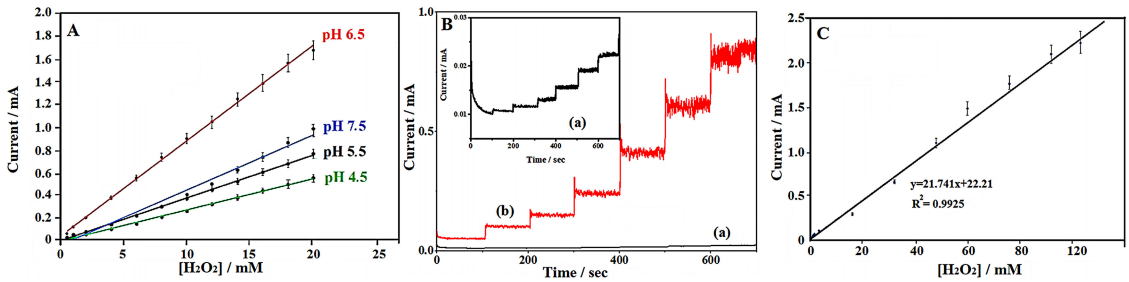

Fig. 6. **(A)** Linear dependence of the response the current *vs.* the H_2O_2 concentration as a function of the pH of PBS (4.5, 5.5, 6.5, 7.5) for P2AB/AuNPs/PGE **(B)** Amperometric *i-t* curves obtained from different concentration of H_2O_2 in 100 mM PBS of pH 6.5 at −0.8 V for (a) P2AB/PGE (b) P2AB/AuNPs/PGE (inset is enlarged Figure 6B (a)) **(C)** Calibration for linearity range of H_2O_2 concentration over P2AB/AuNPs/PGE with error bars (Error bars indicate the standard error of the mean (n = 3)).

current increases with increasing scan rate for P2AB/AuNPs/PGE. Also, it is linearly proportional to the square root of scan rate over a range from 10 to 300 mV s^{-1} (Figure 5B), indicating that the electrochemical response of the P2AB/AuNPs/PGE electrode is a typical diffusion-controlled process.

3.2.2 Amperometric Response of the P2AB/AuNPs/PGE to H_2O_2

Considering the response of bare electrode to H_2O_2 in the PBS solution (Figure 5 (c)), amperometric responses were studied at the potentials between −0.8 V and −0.4 V using P2AB/AuNPs/PGE by amperometric *i-t* curves. The better responding potential was determined as −0.8 V, and it was preferred as an applied potential for determination of H_2O_2. The pH effect of the P2AB/AuNPs/PGE was also investigated for catalytic activity to the H_2O_2 reduction. The current values were plotted against the bulk concentration of H_2O_2 with error bars (Figure 6A). Notably, the slope of calibration curve increases up to pH 6.5 and then decreases again (at pH 7.5). Therefore, the optimum supporting electrolyte medium was determined as 100 mM PBS of pH 6.5.

The current response of P2AB/AuNPs/PGE in the linear range was investigated by successive addition of H_2O_2 with increasing concentrations into 100 mM PBS of pH 6.5 at the applied potential of −0.8 V (Figure 6B (b)). When the response of P2AB homopolymer coated PGE compared to that of P2AB/AuNPs/PGE (Figure 6B (a)), a dramatic current increase was observed for P2AB/AuNPs/PGE. Additionally, P2AB/AuNPs/PGE had a short response time about 6 seconds and an equal current step. Such fast response was attributed to a rapid electron transfer between H_2O_2 and P2AB/AuNPs/PGE. Equal current steps indicate the stable catalytic properties of the modified electrode to H_2O_2. The steady state current values were plotted against the bulk concentration of H_2O_2 with error bars using P2AB/AuNPs/PGE (Figure 6C). This electrode has a detection limit of 3.67×10^{-5} M estimated at a signal to noise ratio of 3. The current response was linear with respect to H_2O_2 concentration over the range from 0.06 to 100 mM ($R^2=0.992$) with a sensitivity of 0.0395 A/M. The validation parameters obtained for P2AB/AuNPs/PGE were summarized in

Table 1 (A). The performance of P2AB/AuNPs/PGE was summarized comparatively with other H_2O_2 sensors based on AuNP modified electrodes in the literature (Table S2). Accordingly, although the LOD of the fabricated electrode could not be significantly improved, a large linear range (0.06 mM–100 mM) was obtained that responded to the high H_2O_2 concentration. The long-term stability of the P2AB/AuNPs electrode was investigated by storing it at room temperature in the atmosphere. The current response to 1.00 mM H_2O_2 was the same for three days and maintained more 53 % of its initial value after ten days.

Table 1. **(A)** Regression data of the calibration curve for assay of H_2O_2 by P2AB/AuNPs/PGE **(B)** Determination of H_2O_2 in real sample (n = 3).

(A) Calibration parameters of P2AB/AuNPs/PGE	
Slope of calibration curve, (A/M)	0.0395
Intercept (A)	1.18×10^{-5}
SD (standard deviation) of calibration (A)	1.20×10^{-6}
SD of slope, (A/M)	1.68×10^{-3}
SD of intercept, A	4.836×10^{-7}
Limit of detection (LOD) (M)	3.67×10^{-5}
Limit of quantification (LOQ) (M)	1.22×10^{-4}
Regression coefficient, R^2	0.992

(B) Sample	Added/mM	Recovery/%	RSD/% (n = 3)
a	1.5	110	3.5
b	3.0	105	9.1

For the selectivity test of P2AB/AuNPs/PGE, the interfering electroactive substances were, ascorbic acid, uric acid, glucose, and dopamine, selected in a similar manner to those reported in the literature [7c,24]. The effect of substances on the response of modified electrode is presented in Figure 7. At an applied potential of −0.8 V, 50.0 mM concentration of glucose, ascorbic acid, dopamine and uric acid cause negligible interference on the detection of H_2O_2 in 100 mM PBS of pH 6.5.

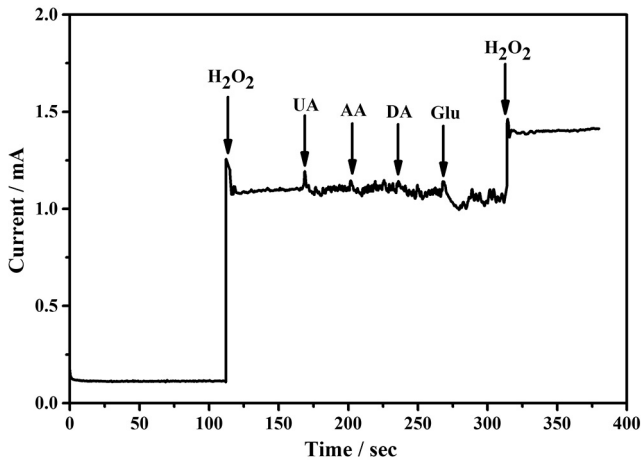

Fig. 7. Effect of interfering species on the response current of the H_2O_2 sensor based on P2AB/AuNPs /PGE in 100 mM PBS at pH 6.5.

To confirm the validation of P2AB/AuNPs/PGE in the detection of H_2O_2 in real samples, the hair dye oxidant sample (3 %) containing the specific concentrations of H_2O_2 was added to PBS and analyzed under optimum conditions obtained above by using the standart addition technique. As seen in Table 1B, the prepared electrode shows good recovery for determination of different concentrations of H_2O_2.

4 Conclusions

Poly(2-aminophenylbenzimidazole) (P2AB) film with gold nanoparticles (AuNPs) coated pencil graphite electrode (PGE) was deposited by cyclic voltammetry in acetonitrile solution by a one-step route. Briefly, $HAuCI_4$ was reduced to AuNPs in the presence of partially protonated 2-aminophenylbenzimidazole monomer in acetonitrile. AuNPs facilitated the electron transfer process, which means that more polymer deposited on the PGE. After optimization and characterization studies, the enzyme-free analysis of H_2O_2 was examined by using P2AB/AuNPs/PGE. It is determined that the sensor efficiently catalyzes the reduction of H_2O_2. The sizeable electroactive surface area of P2AB/AuNPs/PGE improves the analytical performance of sensor. Consequently, P2AB/AuNPs/PGE can be used to as an alternative for non-enzymatic H_2O_2 determination with a low detection limit (3.67×10^{-5} M), wide linear range (0.060 to 100 mM) and easy preparation. In future studies, this electrode can be applied to various biological and environmental studies for analytical determination.

Acknowledgements

The authors would like to thank the financial support from the Hacettepe University Scientific Research Unit (014 D12 601 001-805).

References

[1] a) U. Lange, N. V. Roznyatovskaya, V. M. Mirsky, *Anal. Chim. Acta* **2008**, *614*, 1–26; b) A. K. Sarma, P. Vatsyayan, P. Goswami, S. D. Minteer, *Biosens. Bioelectron.* **2009**, *24*, 2313–2322.

[2] S. Poorahong, C. Thammakhet, P. Thavarungkul, P. Kanatharana, *Pure Appl. Chem.* **2012**, *84*, 2055–2063.

[3] a) A. R. El, H. Y. Aboul-Enein, *Mini-Rev. Med. Chem.* **2013**, *13*, 399–407; b) S. Yadav, B. Narasimhan, *Anti-Cancer Agents Med. Chem.* **2016**, *16*, 1403–1425; c) X. Wang, Y. Wan, Y. Zeng, Y. Gu, *Int. J. Electrochem. Sci.* **2012**, *7*, 2403–2415; d) K. Hwang, J.-H. Kim, S.-Y. Kim, H. Byun, *Energies* **2014**, *7*, 1721–1732.

[4] S. Taj, S. Sankarapapavinasam, M. Ahmed, *J. Appl. Polym. Sci.* **2000**, *77*, 112–115.

[5] a) S. Samms, S. Wasmus, R. Savinell, *J. Electrochem. Soc.* **1996**, *143*, 1225–1232; b) I. Yamaguchi, K. Osakada, T. Yamamoto, *Macromolecules* **1997**, *30*, 4288–4294.
[6] a) P. Staiti, M. Minutoli, S. Hocevar, *J. Power Sources* **2000**, *90*, 231–235; b) P. Mustarelli, E. Quartarone, S. Grandi, A. Carollo, A. Magistris, *Adv. Mater. (Weinheim, Ger.)* **2008**, *20*, 1339–1343.
[7] a) B. E. Watt, A. T. Proudfoot, J. A. Vale, *Toxicol. Rev.* **2004**, *23*, 51–57; b) Y.-X. Liu, R. Devasenathipathy, C. Yang, S.-F. Wang, *Ionics* 1–9; c) S. Karakaya, Y. Dilgin, *Electroanalysis* **2017**, *29*, 1626–1634; d) A. Benvidi, M. T. Nafar, S. Jahanbani, M. D. Tezerjani, M. Rezaeinasab, S. Dalirnasab, *Mater. Sci. Eng. C* **2017**, *75*, 1435–1447.
[8] a) J. Huang, Y. Zhu, H. Zhong, X. Yang, C. Li, *ACS Appl. Mater. Interfaces* **2014**, *6*, 7055–7062; b) F. Wang, S. Hu, *Microchim. Acta* **2009**, *165*, 1–22; c) J. Wang, *Microchim. Acta* **2012**, *177*, 245–270.
[9] a) S. Chen, R. Yuan, Y. Chai, L. Zhang, N. Wang, X. Li, *Biosens. Bioelectron.* **2007**, *22*, 1268–1274; b) C. Yu, L. Wang, W. Li, C. Zhu, N. Bao, H. Gu, *Sensors Actuators B: Chem.* **2015**, *211*, 17–24; c) C.-J. Gu, F.-Y. Kong, Z.-D. Chen, D.-H. Fan, H.-L. Fang, W. Wang, *Biosens. Bioelectron.* **2016**, *78*, 300–307.
[10] a) H. Zhu, A. Sigdel, S. Zhang, D. Su, Z. Xi, Q. Li, S. Sun, *Angew. Chem.* **2014**, *126*, 12716–12720; *Angew. Chem. Int. Ed.* **2014**, *53*, 12508–12512; b) S. Guo, L. Xu, B. Xu, Z. Sun, L. Wang, *Analyst* **2015**, *140*, 820–826.
[11] a) Y. Gong, X. Chen, Y. Lu, W. Yang, *Biosens. Bioelectron.* **2015**, *66*, 392–398; b) M.-R. Zhang, X.-Q. Chen, G.-B. Pan, *Sensors Actuators B: Chem.* **2017**, *240*, 142–147; c) L. Wang, M. Deng, G. Ding, S. Chen, F. Xu, *Electrochim. Acta* **2013**, *114*, 416–423.
[12] a) A. Ayati, A. Ahmadpour, F. F. Bamoharram, B. Tanhaei, M. Manttari, M. Sillanpaa, *Chemosphere* **2014**, *107*, 163–174; b) J. C. Martínez, N. A. Chequer, J. L. González, T. Cordova, *Nanoscience and Nanotechnology* **2013**, *2*, 184–189.
[13] C. Krishnaraj, P. Muthukumaran, R. Ramachandran, M. D. Balakumaran, P. T. Kalaichelvan, *Biotechnol Rep (Amst)* **2014**, *4*, 42–49.
[14] S. Pourbeyram, K. Mehdizadeh, *J. Food Drug Anal.* **2016**, *24*, 894–902.
[15] B. P. Nethravathi, K. N. Mahendra, K. R. K. Reddy, *J. Porous Mater.* **2010**, *18*, 389–397.
[16] A. Shabanikia, M. Javanbakht, H. S. Amoli, K. Hooshyari, M. Enhessari, *Electrochim. Acta* **2015**, *154*, 370–378.
[17] J. A. Asensio, S. Borrós, P. Gómez-Romero, *J. Polym. Sci. Part A* **2002**, *40*, 3703–3710.
[18] X. Du, Y. Xu, L. Xiong, Y. Bai, J. Zhu, S. Mao, *J. Appl. Polym. Sci.* **2014**, *131*, n/a-n/a.
[19] S. Selvasekarapandian, R. Baskaran, O. Kamishima, J. Kawamura, T. Hattori, *Spectrochim. Acta. Part A Mol. Biomol. Spectrosc.* **2006**, *65*, 1234–1240.
[20] S. Mohan, N. Sundaraganesan, J. Mink, *Spectrochim. Acta. Part A Mol. Biomol. Spectrosc.* **1991**, *47*, 1111–1115.
[21] F. Conti, A. Majerus, V. Di Noto, C. Korte, W. Lehnert, D. Stolten, *Phys. Chem. Chem. Phys.* **2012**, *14*, 10022–10026.
[22] A. Valiūnienė, A. I. Rekertaitė, A. Ramanavičienė, L. Mikoliūnaitė, A. Ramanavičius, *Colloids Surf. Physicochem. Eng. Aspects* **2017**, *532*, 165–171.
[23] a) F. Meng, X. Yan, J. Liu, J. Gu, Z. Zou, *Electrochim. Acta* **2011**, *56*, 4657–4662; b) R. Liu, S. Li, X. Yu, G. Zhang, S. Zhang, J. Yao, B. Keita, L. Nadjo, L. Zhi, *Small* **2012**, *8*, 1398–1406.
[24] a) H. Razmi, R. Mohammad-Rezaei, H. Heidari, *Electroanalysis* **2009**, *21*, 2355–2362; b) H. Liu, X. Chen, L. Huang, J. Wang, H. Pan, *Electroanalysis* **2014**, *26*, 556–564; c) C. Revathi, R. R. Kumar, *Electroanalysis* **2017**, *29*, 1481–1489; d) M. Li, C. Deng, C. Chen, L. Peng, G. Ning, Q. Xie, S. Yao, *Electroanalysis* **2006**, *18*, 2210–2217.

Received: September 18, 2018
Accepted: October 19, 2018
Published online on November 13, 2018

